

# The space density of magnetic cataclysmic variables

Magaretha L. Pretorius,<sup>1,2\*</sup> Christian Knigge<sup>2\*</sup> and Axel D. Schwope<sup>3\*</sup>

<sup>1</sup>*European Southern Observatory, Alonso de Córdova 3107, Vitacura, Santiago, Chile*

<sup>2</sup>*School of Physics and Astronomy, University of Southampton, Highfield, Southampton SO17 1BJ, United Kingdom*

<sup>3</sup>*Leibniz-Institut für Astrophysik Potsdam, An der Sternwarte 16, 14482 Potsdam, Germany*

15 October 2018

## ABSTRACT

We use the complete, X-ray flux-limited *ROSAT* Bright Survey (RBS) to measure the space density ( $\rho$ ) of magnetic cataclysmic variables (mCVs). The survey provides complete optical identification of all sources with count rate  $> 0.2 \text{ s}^{-1}$  (corresponding to  $F_X \gtrsim 2 \times 10^{-12} \text{ erg cm}^{-2} \text{ s}^{-1}$ ) over half the sky ( $|b| > 30^\circ$ ), and detected 6 intermediate polars (IPs) and 24 polars. If we assume that the 30 mCVs included in the RBS are representative of the intrinsic population, the space density of mCVs is  $8_{-2}^{+4} \times 10^{-7} \text{ pc}^{-3}$ . Considering polars and IPs separately, we find  $\rho_{\text{polar}} = 5_{-2}^{+3} \times 10^{-7} \text{ pc}^{-3}$  and  $\rho_{\text{IP}} = 3_{-1}^{+2} \times 10^{-7} \text{ pc}^{-3}$ . Allowing for a 50% high-state duty cycle for polars (and assuming that these systems are below the RBS detection limit during their low states) doubles our estimate of  $\rho_{\text{polar}}$  and brings the total space density of mCVs to  $1.3_{-0.4}^{+0.6} \times 10^{-6} \text{ pc}^{-3}$ . We also place upper limits on the sizes of faint (but persistent) mCV populations that might have escaped detection in the RBS. Although the large uncertainties in the  $\rho$  estimates prevent us from drawing strong conclusions, we discuss the implications of our results for the evolutionary relationship between IPs and polars, the fraction of CVs with strongly magnetic white dwarfs (WDs), and for the contribution of mCVs to Galactic populations of hard X-ray sources at  $L_X \gtrsim 10^{31} \text{ ergs}^{-1}$ . Our space density estimates are consistent with the very simple model where long-period IPs evolve into polars and account for the whole short-period polar population. We find that the fraction of WDs that are strongly magnetic is not significantly higher for CV primaries than for isolated WDs. Finally, the space density of IPs is sufficiently high to explain the bright, hard X-ray source population in the Galactic Centre.

**Key words:** binaries – stars: cataclysmic variables, – X-rays: binaries – methods: observational, statistical.

## 1 INTRODUCTION

Cataclysmic variables (CVs) are interacting binary stars in which a white dwarf (WD) accretes matter from a low-mass, Roche-lobe-filling companion. In around 20% of known CVs, the magnetic field of the WD is sufficiently strong to control at least the inner part of the accretion flow; these magnetic CVs (mCVs) are divided into two classes, namely polars and intermediate polars (IPs). The defining property of a polar is that the WD is locked in synchronous rotation with the binary orbit, while IPs have WD spin periods typically much shorter than the orbital period ( $P_{\text{orb}}$ ).

In many ways, the formation and evolution of magnetic and non-magnetic CVs is thought to be similar. Both

types of systems form through common envelope (CE) evolution, evolve first from long to short  $P_{\text{orb}}$  because of angular momentum loss (AML), and eventually experience period bounce, when the thermal time-scale of the donor becomes longer than its mass loss time-scale. In fact, the main proposed difference between the evolution of mCVs and non-magnetic CVs affects only the polars. In these systems, magnetic braking (MB), which is thought to be the dominant AML mechanism for most CVs above the period gap, is likely to be suppressed (e.g. Li & Wickramasinghe 1998; Townsley & Gänsicke 2009). The  $P_{\text{orb}}$  distribution of mCVs is broadly in line with these ideas: if polars and IPs are considered jointly, their  $P_{\text{orb}}$  distribution is very similar to that of non-magnetic CVs, showing both a period gap in the range  $2 \text{ hr} \lesssim P_{\text{orb}} \lesssim 3 \text{ hr}$  and a period minimum at around  $P_{\text{orb}} \simeq 80 \text{ min}$  (see Fig. 1).

However, there are at least three important open ques-

\* E-mail: m.pretorius@soton.ac.uk (MLP); c.knigge@soton.ac.uk (CK); aschwope@aip.de (ADS)

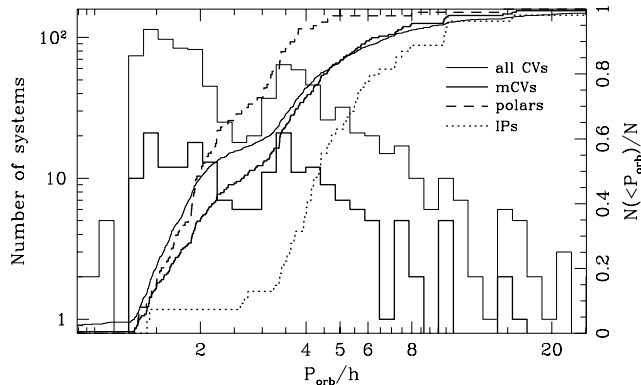


**Figure 1.** The orbital period distribution of all CVs (fine histogram), and mCVs (bold histogram). Cumulative distributions are also shown for polars (dashed histogram) and IPs (dotted histogram). Almost all IPs are found at long  $P_{orb}$ , while most polars are short- $P_{orb}$  systems. Although the period distribution of mCVs shows a period gap, it is less pronounced than for non-magnetic CVs. The periods used here are taken from version 7.18 of the catalogue of Ritter & Kolb (2003).

tions concerning the formation, evolution and Galactic abundance of mCVs:

- (i) Is there an evolutionary relationship between IPs and polars?
- (ii) What is the intrinsic fraction of mCVs amongst the general CV population, and can this be reconciled with the incidence of magnetic WDs in the isolated WD population?
- (iii) Do mCVs dominate the total Galactic X-ray source populations above  $L_X \sim 10^{31}$  ergs $^{-1}$ ?

In principle, all of these questions can be addressed empirically, but this requires reliable measurements of the space density of IPs and polars. The goal of the present work is to provide such measurements.

The plan of this paper is as follows. In Section 2, we will provide some additional background on the questions listed above, and discuss previous attempts to measure the space densities of polars and IPs. Our flux-limited, X-ray-selected mCV sample is presented in Section 3, with distance and X-ray luminosity estimates discussed in Section 4 and 5. In Section 6, we describe how we use this sample to calculate space densities, and present our results. The results are discussed in Section 7, and, finally, we list our conclusions in Section 8.

## 2 CONTEXT

### 2.1 The relationship between intermediate polars and polars

It has been known for a long time that most IPs are found above the period gap and most polars below (see Fig. 1). This immediately suggests that IPs may evolve into polars (Chanmugam & Ray 1984; King, Frank & Ritter 1985). This is a physically appealing idea. Whether the WD in a given system will synchronize depends on the strength of the WD’s magnetic field, the orbital separation, and the mass-transfer rate ( $\dot{M}$ ) from the secondary star (with large

magnetic field, small orbital separation, and low  $\dot{M}$  favouring synchronization). Since MB drives much higher mass-transfer rates above the period gap than gravitational radiation (GR) does below, it is plausible that many accreting magnetic WDs may only achieve synchronization once they have crossed the period gap.

There is, however, a serious problem with this attractive scenario. If most IPs evolve into polars, and most polars are the descendants of IPs, their field strengths should be comparable. Yet, empirically, the magnetic fields of the WDs in IPs ( $B_{IP} \lesssim 10$ MG) are systematically weaker than those of the WDs in polars ( $B_{polar} \sim 10 - 100$ MG) (e.g. Chanmugam & Ray 1984; Wickramasinghe, Wu & Ferrario 1991; Lamb & Melia 1987; Schmidt et al. 1996, 2001; Norton, Wynn & Somerscales 2004; Schwope, Schreiber & Szkody 2006; Butters et al. 2009).

There are several possible resolutions to this problem. Perhaps the simplest (in terms of binary evolution) is that the high accretion rates in IPs may partially “bury” the WD magnetic fields, so that the observationally inferred field strengths for these systems are systematically biased low (Cumming 2002). Alternatively, Patterson (1994) points out that it may not be necessary for all (or even most) long-period IPs to evolve into polars in order to account for the entire short-period polar population, since the evolutionary time-scales are so much shorter above the period gap than below. This idea still requires an explanation for the fate of the remaining long-period IPs, although perhaps they simply become unobservable as their accretion flows become clumpy and their luminosity is pushed into the EUV band (Wickramasinghe, Wu & Ferrario 1991). Finally, the opposite view would be that the short-period polar population may be dominated by systems born below the period gap. But in this case, there would have to be a direct link between the WD field strength and the orbital period after emergence from the CE phase (e.g. Tout et al. 2008).

One way to shed light on the relationship between IPs and polars is via their respective space densities. For example, if all long-period IPs evolve into short-period polars, and all short-period polars are the progeny of long-period IPs, then their space densities should be proportional to the evolutionary time-scale associated with these phases. In this particular example, we would predict that  $\rho_{polar}/\rho_{IP} \simeq \tau_{GR}/\tau_{MB} \gg 1$ .

### 2.2 The intrinsic fraction of magnetic CVs

Magnetic systems make up  $\simeq 20\%$  of the known CV population (Ritter & Kolb 2003). At first sight, this is a surprisingly high fraction, given that the strong magnetic fields characteristic of IPs and polars ( $B \gtrsim 10^6$  G) are found in only  $\simeq 10\%$  of isolated WDs (e.g. Kawka et al. 2007; Külebi et al. 2009). If these numbers are representative of the intrinsic incidence of magnetism amongst CVs and single WDs, the difference between them would have significant implications: either strong magnetic fields would have to favour the production of CVs, or some aspect(s) of pre-CV evolution would have to favour the production of strong magnetic fields.

A model along the latter lines was recently proposed by Tout et al. (2008). They argue that all strongly magnetic WDs are the product of binary evolution, and that

the observed strong fields develop during the CE phase. In this picture, mCVs are associated with CE events that produce very close binary systems (which are then brought into contact by MB or GR), while isolated magnetic WDs are produced when two degenerate cores undergo a complete merger during the CE phase.

However, it is actually by no means clear yet that magnetism is really more common in CV primaries than in isolated WDs. The main problem is that the observed fraction of magnetic systems amongst known CVs is almost certainly affected by serious selection biases. For example, since mCVs are known to be relatively X-ray bright, they are likely to be over-represented in X-ray-selected samples. Conversely, polars, in particular, are relatively faint in optical light (since they do not contain optically bright accretion disks), so they are likely to be under-represented in optically-selected samples. Given that the overall CV sample is a highly heterogeneous mixture of X-ray-, optical- and variability-selected sub-samples (which also usually lack clear flux limits), it is very difficult to know how the observed fraction of mCVs relates to the intrinsic fraction of magnetic WDs in CVs.

### 2.3 Galactic X-ray Source Populations

There have been many attempts to determine the make-up and luminosity function of Galactic X-ray source populations in a variety of environments, ranging from the Milky Way as a whole (e.g. Sazonov et al. 2006), the Galactic Centre (e.g. Muno et al. 2004, 2006, 2009), the Galactic Ridge (e.g. Revnivtsev et al. 2006; Krivonos et al. 2007; Hong et al. 2012), and even globular clusters (e.g. Heinke et al. 2005). Remarkably, in all of these environments, mCVs have been proposed as the dominant population of X-ray sources above  $L_X \gtrsim 10^{31} \text{ erg s}^{-1}$ .

However, in most of the above studies, the breakdown of the observed X-ray source samples into distinct populations is subject to considerable uncertainty. In general, only a small fraction of the sources have optical counterparts and/or properties that would permit a clear classification. Thus, for the most part, identifications of observed sources with physical populations have to rely on gross properties (such as X-ray colours and luminosities) and statistical comparisons of observed and expected number counts. The local space densities of the relevant populations are arguably the most important ingredient in these comparisons. In effect, the question being asked is whether the extrapolation of the local space density to the environment being investigated can account for the observed number of sources seen there. In the case of mCVs, such extrapolations are difficult, primarily because the local space densities are rather poorly constrained.

### 2.4 The Space Density of Magnetic CVs: Previous Work

#### 2.4.1 Polars

Estimates for the space density of polars include  $\sim 3.5 \times 10^{-7} \text{ pc}^{-3}$  (Patterson 1984),  $\sim 3 \times 10^{-7} \text{ pc}^{-3}$  (Warner 1995),  $\sim 5 \times 10^{-7} \text{ pc}^{-3}$  (Cropper 1990), and  $1.3 \times 10^{-6} \text{ pc}^{-3}$  (Araujo-Betancor et al. 2005). As emphasized particularly in the last of these studies, all of these numbers are, strictly

speaking, lower limits, because they are effectively based on the number of systems observed within a particular distance cut-off.

Thomas & Beuermann (1998) derive an estimate of  $\rho_{\text{polar}} \simeq 6.1 \times 10^{-7} \text{ pc}^{-3}$  from the sample of polars detected by *ROSAT* (see also Beuermann & Schwope 1994). However, they also note that, allowing for incompleteness, the space density could be as high as  $1.2 \times 10^{-6} \text{ pc}^{-3}$  for short-period polars and  $1.7 \times 10^{-7} \text{ pc}^{-3}$  for long-period polars. Ramsay et al. (2004b) discuss the issue of incompleteness in observed samples, particularly that arising from the extended low-states exhibited by polars.

#### 2.4.2 Intermediate Polars

Fewer estimates are available for the space density of IPs. Warner (1995) gives  $\rho_{IP} \sim 3 \times 10^{-8} \text{ pc}^{-3}$ , while Revnivtsev et al. (2008) find  $\rho_{IP} \simeq 1.2 \times 10^{-7} \text{ pc}^{-3}$ , from a sample of CVs detected by *INTEGRAL*. The scarcity of space density estimates for IPs is particularly problematic, because it is IPs, rather than polars, which are often assumed to be the dominant bright hard X-ray source population in many Galactic environments (see Section 7.3).

## 3 THE FLUX-LIMITED CV SAMPLE

Given that we do not yet have a useful volume-limited CV sample, the most suitable sample to use for statistical studies is a purely flux-limited one (e.g. Pretorius et al. 2007a).

In two previous papers (Pretorius et al. 2007b; Pretorius & Knigge 2012) we presented constraints on the space density and X-ray luminosity function of non-magnetic CVs, based on the *ROSAT* Bright Survey (RBS; Schwope et al. 2000), as well as on the deeper, but smaller area *ROSAT* North Ecliptic Pole (NEP) survey (e.g. Gioia et al. 2003; Henry et al. 2006). Here, we use the RBS to derive the corresponding observational constraints on the mCV population.

While several non-magnetic CVs are known to have very faint X-ray luminosities, mCVs are expected to be intrinsically brighter in X-rays, because of the almost radial accretion flow (polars in particular also have higher soft X-ray to optical flux ratios than non-magnetic CVs, explaining why so many were first discovered by *ROSAT*; see fig. 2 of Beuermann & Thomas 1993). This means that the bright flux limit of the RBS is not as important a concern when studying mCVs.

The RBS is a flux-limited part of the *ROSAT* All-Sky Survey (RASS; see Voges et al. 1999 and Voges et al. 2000), consisting of bright (count rate  $> 0.2 \text{ s}^{-1}$ ), high Galactic latitude ( $|b| > 30^\circ$ ) sources. It has complete optical follow-up (Schwope et al. 2000; Schwope et al. 2002), and includes 30 mCVs — 6 IPs and 24 polars. Assuming a 30 keV thermal bremsstrahlung spectrum, and a 30 eV blackbody spectrum (see Section 5), both with  $N_H = 10^{20} \text{ cm}^{-2}$ , the limiting count rate corresponds to flux limits of  $F_X \gtrsim 3 \times 10^{-12} \text{ erg cm}^{-2} \text{ s}^{-1}$  and  $2 \times 10^{-12} \text{ erg cm}^{-2} \text{ s}^{-1}$ , respectively, in the 0.12–2.48 keV band.

In Table 1 we list the 30 mCVs that make up our flux-limited sample. It has been suggested that two more CVs detected in the RBS are magnetic; these are TW

Pic (see Mouchet et al. 1991; Patterson & Moulden 1993; Norton et al. 2000) and V405 Peg (Thorstensen et al. 2009). We do not include these two systems here, since there is no conclusive evidence of a magnetic nature for either of them. On the other hand, CC Scl was until recently classified as a normal SU UMa star, but has now been shown to be an IP (Woudt et al. 2012); we therefore include it in our mCV sample<sup>1</sup>.

## 4 DISTANCE ESTIMATES

We require distance estimates for all mCVs in the sample. Where possible, we use published distances, based on either trigonometric parallax, or photometric parallax of the WD or donor star. In most cases, however, the best distance estimates we can obtain are quite uncertain. This will be the most important limit on the precision of our space density measurement. The estimates we use are listed in Table 1, and we provide more information below.

### 4.1 Systems with reliable distance estimates

#### 4.1.1 Trigonometric parallax

The IPs EX Hya and TV Col, and the polar EF Eri have very reliable distance estimates from parallax measurements (McArthur et al. 2001; Beuermann et al. 2003; Thorstensen 2003).

#### 4.1.2 Photometric parallax

Several more systems have reliable distance estimates from photometric parallax of one of the stellar components. These are based on, e.g., the detection of donor star features in the optical or near-IR spectrum (from which the donor's contribution to the total flux in a given band can be estimated), or FUV observations in a low state, where the WD dominates the flux.

Based on donor star features in the near-IR spectrum of DO Dra, Mateo, Szkody, & Garnavich (1991) find a distance of  $155 \pm 35$  pc. This is very close agreement with an estimate from the FUV detection of the WD (Hoard et al. 2005).

Araujo-Betancor et al. (2005) find a distance of  $163_{-26}^{+18}$  for BL Hyi, from a FUV detection of the WD (several more estimates, all consistent with this, have been derived from detections of the donor star; see Visvanathan, Bessell, & Wickramasinghe 1984; Beuermann et al. 1985, Glenn et al. 1994, Beuermann 2000).

HU Aqr is a deeply eclipsing polar; Ciardi et al. (1998) find  $K = 15.3(1)$  in eclipse, and note that the eclipse is probably total. Knowing the orbital period and the spectral type of the secondary (M4.5; Schwope, Thomas, & Beuermann

1993), we can use the predicted absolute magnitude of the star (Knigge 2006; Knigge et al. 2011) to find a distance of  $290_{-80}^{+110}$  pc, in line with the  $\sim 250$  pc reported by Schwope, Thomas, & Beuermann (1993). The smaller distance estimates of Ciardi et al. (1998) and Sproats, Howell, & Mason (1996) result from assuming a later spectral type. Gänsicke (1999) also estimated  $\sim 180$  pc from low-state UV data, but he notes that there was still some accretion during the observation.

Finally, Reinsch et al. (1994) estimate a distance of  $300 \pm 60$  pc for UW Pic, and Schwarz et al. (1998) find  $620 \pm 100$  pc for AI Tri, both also from the photometric parallax of the donor.

### 4.2 Systems for which only less reliable estimates are possible

For the remaining 22 systems, we have to turn to a less direct method of estimating distances. The donor star is expected to be responsible for a large fraction of the near- and mid-IR flux of a CV. Therefore, even in cases where the contribution of the donor star to a system's IR light is not known, it is possible to use IR photometry to obtain rough distance estimates. This is similar to the method of Bailey (1981), although we will use the predicted absolute donor magnitudes of Knigge (2006) and Knigge et al. (2011). Below, we will first estimate the average contribution of the donor to the near- and mid-IR flux of mCVs, and then use this to estimate distances for most of the systems in our sample<sup>2</sup>.

#### 4.2.1 Finding the average mCV donor contribution to near- and mid-IR flux

Knigge (2006) and Knigge et al. (2011) give the average differences between the absolute *JHK* magnitudes of CV donors predicted by their semi-empirical sequence and the measured absolute magnitudes of a sample of CVs (consisting mostly of non-magnetic systems, but including also a few mCVs) with parallax distance estimates. This gives an estimate of the typical donor contribution to the flux in these bands, and, together with an apparent IR magnitude, can be used to obtain a rough distance estimate (as well as a robust lower limit on the distance).

In order to repeat this for mCVs alone, we use a sample of 23 magnetic systems with orbital periods below 6 hours and reliable distance estimates. The distances are based on trigonometric parallax (for 4 IPs and 5 polars), photometric parallax of the WD (5 polars), or photometric parallax the donor (1 IP and 8 polars). Not surprisingly, we find that the typical donor contribution to the IR light is similar for IPs and non-magnetic CVs (systems with discs), and smaller for polars. Therefore, we group IPs and non-magnetic CVs together, and consider the sample of polars separately. Furthermore, we decided to omit the polars with published distances from photometric parallax of the donor<sup>3</sup>; this means

<sup>1</sup> Although we previously incorrectly included CC Scl in the RBS non-magnetic CV sample, it made only a very small contribution to our earlier estimate of the non-magnetic CV space density (Pretorius & Knigge 2012), so that the result presented there was not significantly affected. It is however important to include CC Scl here, because the total space density of magnetic systems is smaller.

<sup>2</sup> Ak et al. (2008) present another method of estimating distances from near-IR photometry, and also give distances for several of the mCVs in this sample.

<sup>3</sup> Because it is possible that in these systems, the contribution to the IR light of, e.g., the accretion flow, is systematically low, given

**Table 1.** The 30 mCVs detected in the RBS, together with their subtype (polar or IP), orbital periods, Galactic latitudes, *ROSAT* PSPC count rates, distances, and X-ray luminosities. The fraction of the total mCV space density contributed by each system ( $\rho_j/\rho_0$ ) is given in the 8th column (this ignores all errors, although uncertainties are correctly accounted for later; see Section 6.1). References are for the classification as a magnetic CV,  $P_{orb}$ , and published distances, where available. Note that the distance and  $L_X$  estimates for CD Ind, IW Eri, CV Hyi, and FH UMa are very uncertain (see Section 4.2.3 and 6.3.1).

System	RBS#	Type	$P_{orb}/h$	$b$	count rate/s $^{-1}$	$d/pc$	$\log(L_X/erg\ s^{-1})$	$\rho_j/\rho_0$	References
CC Scl	1969	IP	1.402	-68.7°	0.28(6)	200 $^{+110}_{-70}$	31.3(4)	0.089	1,2,3
EX Hya	1173	IP	1.638	+33.6°	5.4(3)	64.5 ± 1.2	31.59(4)	0.043	4,5
AO Psc	1914	IP	3.591	-53.3°	0.37(4)	330 $^{+180}_{-120}$	32.2(4)	0.048	6,7
DO Dra	1022	IP	3.969	+44.5°	0.59(3)	155 ± 35	31.4(2)	0.119	8,9
TV Col	655	IP	5.486	-30.6°	0.36(4)	370 $^{+17}_{-15}$	32.22 $^{+0.08}_{-0.09}$	0.046	10,11
EI UMa	713	IP	6.434	+37.4°	0.57(4)	750 $^{+100}_{-200}$	33.2 $^{+0.1}_{-0.3}$	0.021	12,13
CV Hyi	213	AM	1.297	-50.7°	0.28(4)	550 $^{+450}_{-250}$	32.3(6)	0.013	14
V4738 Sgr	1678	AM	1.300	-33.9°	0.33(4)	250 $^{+90}_{-70}$	31.8 $^{+0.4}_{-0.5}$	0.035	14
EV UMa	1219	AM	1.328	+63.1°	1.86(6)	690 $^{+270}_{-190}$	33.3(3)	0.003	15,16
GG Leo	842	AM	1.331	+49.0°	1.1(1)	170 $^{+90}_{-60}$	31.5(4)	0.058	17,18
FH UMa	904	AM	1.336:	+48.4°	0.26(2)	590 $^{+480}_{-270}$	32.0(6)	0.023	19
EF Eri	398	AM	1.350	-57.4°	6.2(3)	163 $^{+66}_{-50}$	32.0 $^{+0.3}_{-0.4}$	0.023	20,21
IW Eri	541	AM	1.452:	-40.6°	0.23(3)	270 $^{+230}_{-120}$	31.6(6)	0.048	22
EU UMa	1039	AM	1.502	+76.3°	3.3(2)	240 $^{+90}_{-60}$	32.4(3)	0.010	18,23,24
EQ Cet	206	AM	1.547	-80.9°	0.34(3)	270 $^{+130}_{-90}$	31.4(4)	0.077	22,25
V393 Pav	1664	AM	1.647	-31.3°	0.90(7)	340 $^{+170}_{-110}$	32.4(5)	0.011	26
EG Lyn	696	AM	1.656	+34.5°	0.25(3)	470 $^{+230}_{-160}$	32.4(4)	0.010	22,27
RS Cae	599	AM	1.699:	-39.1°	1.20(8)	880 $^{+330}_{-240}$	33.0(3)	0.004	28
CD Ind	1735	AM	1.848	-41.4°	0.38(4)	350 $^{+140}_{-100}$	31.7(4)	0.044	29,30
BL Hyi	232	AM	1.894	-48.6°	2.8(2)	163 $^{+18}_{-26}$	31.7(2)	0.037	31,32,33,34,35
EK UMa	911	AM	1.909	+55.2°	1.11(5)	590 $^{+340}_{-210}$	32.6(4)	0.008	36,37,38
AN UMa	938	AM	1.914	+62.1°	1.77(7)	300 $^{+150}_{-100}$	31.9(4)	0.029	39,40,41
V1007 Her	1646	AM	1.999	+33.3°	0.24(2)	560 $^{+280}_{-180}$	32.3(5)	0.011	42
HU Aqr	1724	AM	2.084	-32.6°	0.81(7)	290 $^{+110}_{-80}$	32.2 $^{+0.4}_{-0.5}$	0.015	43,44,45
UW Pic	658	AM	2.223	-32.7°	0.73(9)	300 ± 60	31.9(3)	0.028	46,47
RX J0859	734	AM	2.397	+30.9°	0.23(3)	530 $^{+260}_{-180}$	32.6(4)	0.008	48,49,50
CW Hyi	324	AM	3.030	-45.9°	0.26(4)	500 $^{+250}_{-170}$	32.4(4)	0.035	22
RX J1610	1563	AM	3.176	+37.3°	0.36(4)	380 $^{+190}_{-120}$	32.1(5)	0.050	22,51
1RXS J231603	1973	AM	3.491	-58.6°	1.10(9)	460 $^{+170}_{-120}$	32.8(3)	0.026	51,52
AI Tri	274	AM	4.602	-30.3°	0.54(5)	620 ± 100	32.5(3)	0.031	53

References: 1. Woudt et al. (2012); 2. Chen et al. (2001); 3. Tappert et al. (2004); 4. Sterken et al. (1983); 5. Beuermann et al. (2003); 6. Patterson & Price (1981); 7. Patterson (1984); 8. Mateo, Szkody, & Garnavich (1991); 9. Hoard et al. (2005); 10. Hellier (1993); 11. McArthur et al. (2001); 12. Reimer et al. (2008); 13. Thorstensen (1986); 14. Burwitz et al. (1997); 15. Osborne et al. (1994); 16. Katajainen et al. (2000); 17. Burwitz et al. (1998); 18. Ramsay et al. (2004a); 19. Singh et al. (1995); 20. Thorstensen (2003); 21. Williams et al. (1979); 22. Schwöpe et al. (2002); 23. Mittaz et al. (1992); 24. Howell et al. (1995); 25. Schwöpe, Schwarz, & Greiner (1999); 26. Thomas et al. (1996); 27. Cao, Wei & Hu (1999); 28. Burwitz et al. (1996); 29. Schwöpe et al. (1997); 30. Ramsay et al. (1999); 31. Araujo-Betancor et al. (2005); 32. Beuermann et al. (1985); 33. Visvanathan, Bessell, & Wickramasinghe (1984); 34. Beuermann (2000); 35. Glenn et al. (1994); 36. Morris et al. (1987); 37. Clayton & Osborne (1994); 38. Beuermann et al. (2009); 39. Krzeminski & Serkowski (1977); 40. Bonnet-Bidaud et al. (1996); 41. Liebert et al. (1982); 42. Greiner, Schwarz & Wenzel (1998); 43. Schwöpe, Thomas, & Beuermann (1993); 44. Ciardi et al. (1998); 45. Sproats, Howell, & Mason (1996). 46. Reinsch et al. (1994); 47. Romero-Colmenero et al. (2003); 48. Beuermann & Burwitz (1995); 49. Beuermann et al. (1999); 50. Gänsicke et al. (2009); 51. Rodrigues et al. (2006); 52. Beuermann & Thomas (1993); 53. Schwarz et al. (1998).

that our average donor contributions for polars are based on a sample of only 10 systems.

For the two samples of CVs with reliable distance estimates (IPs, together with the non-magnetic CVs used by Knigge 2006, and the sample of 10 polars) separately, we calculate the average of the difference between the measured absolute magnitude of the CVs and the absolute magnitude predicted for the donor star at that period by Knigge (2006). We do this for the 2MASS (Skrutskie et al. 2006) *JHK* bands, as well as the 2 shortest wavelength *WISE* (Wright et al. 2010) bands, W1 and W2. On average, the donor stars in polars emit, e.g., around 60% of the *K*-band light (compared to 31%, for the sample of mostly non-magnetic CVs used by Knigge 2006). These results will be presented in more detail in a future paper.

Clearly, a single number cannot describe the donor contribution to the flux in some waveband for all systems and at all  $P_{orb}$ . However, the sequence of Knigge (2006), together with the typical fractions of the near- and mid-IR flux contributed by the donor, should allow us to predict absolute magnitudes to within the errors implied by the CV samples used to find these fractions. We take the error in the predicted absolute near- and mid-IR magnitudes to be the standard deviation of the absolute magnitudes of these two samples from the sequence, after it is offset to include the typical flux contribution from sources other than the donor.

A final caveat is that the donor sequence may not be applicable to long-period polars, because it is based on the masses and radii of donor stars in non-magnetic CVs (which have MB above the orbital period gap, while polars perhaps never experience MB). We are probably safe in ignoring this difficulty, since we use the method for only 3 long-period polars, and since no single distance estimate strongly affects our space density estimate<sup>4</sup>.

#### 4.2.2 Distance estimates relying on the estimated typical donor IR flux contribution

We use the method outlined above to find distance estimates for 18 of the mCVs in the RBS sample. In doing this, we assume that none of these systems are period bouncers, or have evolved donor stars (except for EI UMa, where we adopt an estimate from the literature that allows for this; see below). We include the effect of interstellar extinction in the distance estimates when using 2MASS photometry, but neglect it when using *WISE* mid-IR photometry (extinction estimates for our sources are discussed in Section 5 below). We then find the probability distribution function for the distance to each source, assuming Gaussian errors in predicted absolute magnitudes, apparent magnitudes, and extinction. The distance estimates listed in Table 1 are the median, together with the 1- $\sigma$  confidence interval corresponding to the 16th and 84th percentile points. We briefly discuss individual systems below.

that spectral features of the donor stars are relatively prominent in the optical spectra.

<sup>4</sup> Furthermore, the high mass loss rates of non-magnetic CVs above the period gap cause the donor radius to expand by at most  $\simeq 30\%$  (Patterson et al. 2005; Knigge 2006). The implied  $\simeq 30\%$  distance error is too small to dominate the uncertainty in our estimates.

CC Scl has DN outbursts (as several IPs do), but since it is certainly not a typical DN (besides being an IP, its superoutbursts have unusually low amplitude and short duration), we prefer not to base our distance estimate on the outburst maximum here. We obtain a distance of  $200^{+110}_{-70}$  pc from *WISE* photometry, slightly smaller than the estimate of  $360 \pm 130$  pc that Patterson (2011) finds from the outburst maximum.

The distance of  $330^{+180}_{-120}$  pc that we find for AO Psc using *WISE* photometry is consistent with the estimate of  $\sim 250$  pc obtained by Patterson (1984) from a relation between the strength of emission lines and the absolute magnitude of the disc.

For EI UMa, we adopt the estimate of Reimer et al. (2008), which is based on the same method we use here. Note that it is a tentative estimate because this system has  $P_{orb}$  in the range where the CV population is expected to be dominated by systems with evolved donors (some attempt was made to reflect this in the error; Reimer et al. 2008).

EV UMa was in a high state when it was observed by 2MASS; we therefore use  $K = 19.3(2)$  from Osborne et al. (1994) to obtain  $d = 690^{+270}_{-190}$  pc. Osborne et al. (1994) give a lower limit of 705 pc on the distance to this system.

Ramsay et al. (2004a) find distances of 50–70 pc and 60–80 pc for GG Leo and EU UMa, respectively, from UV data. They note, however, that these are likely underestimates, since some of the UV flux might be from sources other than the WDs. We find larger distances in both these cases (using *WISE* photometry for GG Leo, and the 2MASS *H* measurement for EU UMa). Our estimate of  $d = 170^{+90}_{-60}$  pc for GG Leo is consistent with limits of  $d > 100$  pc (based on the optical spectrum; Burwitz et al. 1998) and  $d < 300$  pc (from the requirement that the implied accretion rate is not unreasonably high; Brinkworth et al. 2007).

We use *WISE* data of V393 Pav to estimate  $d = 340^{+170}_{-110}$  pc, in agreement with the estimate of  $d \sim 350$  pc by Thomas et al. (1996).

V4738 Sgr and RS Cae are not detected by 2MASS or *WISE*; we find  $H = 17.61(9)$  and  $18.1(1)$ , for these two systems, from images obtained with the Infrared Survey Facility (IRSF; see e.g. Glass & Nagata 2000 and Nagayama et al. 2003) at the South African Astronomical Observatory. This gives distance estimates of  $250^{+90}_{-70}$  pc and  $880^{+330}_{-240}$  pc for V4738 Sgr and RS Cae, respectively. Note that although the radial velocity curve of RS Cae is aliased (Burwitz et al. 1996) the uncertainty in period does not significantly affect the distance estimate. From the absence of M star features in the optical spectra, lower limits of  $d > 440$  pc for RS Cae (Burwitz et al. 1996) and  $d > 190$  pc for V4738 Sgr (Burwitz et al. 1997) have been derived.

Clayton & Osborne (1994) report  $K = 16.4(7)$  for EK UMa (which is also not detected by 2MASS or *WISE*), and give a lower limit of  $d > 410$  pc. We use their *K*-band magnitude to estimate  $d = 590^{+340}_{-210}$  pc for this system.

Patterson (1984) estimates  $d \sim 400$  pc for AN UMa (Warner 1995 lists a limit of  $> 270$  pc; see also Liebert et al. 1982 for some discussion on lower distance limits). We find  $300^{+150}_{-100}$  pc, using *WISE* photometry.

For V1007 Her, we use the W1 band of *WISE* to find a distance of  $560^{+280}_{-180}$  pc. Greiner, Schwarz & Wenzel (1998) give a lower limit of  $d > 250$  pc.

We obtain a distance of  $500^{+250}_{-170}$  pc for CW Hyi, again

from the W1-band magnitude. Our estimate is slightly large compared to the distance of  $\sim 250$  pc reported by Schwobe et al. (2002); however, the donor star features are not prominent in the optical spectrum, implying that the estimate of the donor contribution to the optical flux is quite rough (Schwobe et al. 2002).

Our distance estimate of  $380^{+190}_{-120}$  pc for RX J1610.1+0352 (also called RBS 1563) from *WISE* photometry is in good agreement the estimate of 320 pc that Ak et al. (2008) obtain from 2MASS data.

We use the 2MASS *H*-band magnitude of 1RXS J231603.9-052713 (RBS 1973) to find a distance of  $460^{+170}_{-120}$  pc. Rodrigues et al. (2006) have estimated  $\simeq 410$  pc, in agreement with our value, from a model of the optical and infrared flux that includes cyclotron emission and a heated secondary.

There is no published information on the distances of EQ Cet, EG Lyn, and RX J0859.1+0537 (RBS 734). We use *WISE* detections of these 3 systems in our distance estimates.

#### 4.2.3 Systems for which we obtain only very weak distance constraints

We are now left with 4 systems for which estimating distances presents more serious problems. These are CD Ind, IW Eri, CV Hyi, and FH UMa. For CD Ind and IW Eri, the method discussed above produces distance estimates that are inconsistent with other information, while no near- or mid-IR detections are available for CV Hyi and FH UMa. We discuss these systems in turn below. In Section 6.3.1 we will show that these four very poorly constrained distances do not have an important effect on our space density estimate. This is because we are able to place lower limits on the distances, and, in all 4 cases, the resulting upper limit on the contribution of these systems to the total space density is small.

Apparent magnitudes in the 2MASS and *WISE* bands, together with our assumptions about typical donor flux contributions in the IR bands, would imply a distance of roughly 110 pc for CD Ind. However, Schwobe et al. (1997) find no sign of the donor in their optical spectra, and give a lower limit of  $d > 250$ , assuming a donor spectral type of M5.

For IW Eri, *WISE* magnitudes would yield a distance of only about 80 pc, which is inconsistent with its non-detection in 2MASS. We measure  $K > 15.5$  (from the faintest detections in the area around IW Eri), implying  $d > 150$  pc.

Both CD Ind and IW Eri have low- and high photometric states (Schwobe et al. 1997; Schwobe et al. 2002). It is possible that CD Ind was observed in a high state by 2MASS as well as *WISE*, while IW Eri was caught in a high state by *WISE* and in a low state by 2MASS. The high-state optical spectrum of CD Ind shows rising flux towards the red end, interpreted as cyclotron emission caused by a weak magnetic field ( $B \simeq 11$  MG; Schwobe et al. 1997). Therefore, CD Ind likely has unusually large cyclotron emission in the IR, because of its unusually low magnetic field strength.

For CV Hyi and FH UMa, we find lower limits of  $d > 300$  pc and  $d > 320$  pc, respectively, from *WISE* non-

detections. Burwitz et al. (1997) also report  $d > 300$  pc for CV Hyi, based on its optical spectrum.

We can derive conservative upper limits on the distances of these 4 systems from what would be implausible optical luminosities, or even position in the galaxy. However, since such limits are very weak, they are not useful here. It does seem that IW Eri is not very distant, since it has a proper motion of about 45 mas/yr (Monet et al. 2003; Peters 2008). Patterson (2011) finds a tangential velocity of  $39 \pm 5$  km/s for a sample of normal non-magnetic CVs. If we assume that IW Eri comes from a population with the same age, we can tentatively estimate a distance of  $\sim 180$  pc.

For these 4 systems we will simply assume distance distributions that are Gaussian in  $\log(d)$ , with  $\sigma_{\log(d)}$  chosen so that the 16th percentile corresponds to the lower limits given above. Of course this is not correct, but our space density estimate is not strongly affected (see Section 6.3.1).

### 4.3 Possible bias in distance estimates

Distance estimates used here may suffer from the well-known Malmquist (Malmquist 1924; in the case of photometric parallax) and Lutz-Kelker (Lutz & Kelker 1973; for trigonometric parallax) biases. We are not concerned about Lutz-Kelker bias in the parallax measurements of EX Hya, TV Col and EF Eri, because the parallax errors are very small in the first two cases (McArthur et al. 2001; Beuermann et al. 2003), and because the bias was considered by Thorstensen (2003) in the case of EF Eri. This leaves the possibility of Malmquist bias in the photometric parallax distances presented in Section 4.1.2 and 4.2.2. We have checked how large this effect could be, in the same way as described in Pretorius & Knigge (2012). We find that the bias, if present at all (see the more detailed discussion in Pretorius & Knigge 2012), is in each case insignificant.

## 5 X-RAY SPECTRA AND LUMINOSITIES

Polars are luminous soft X-ray sources, and a large number was detected by *ROSAT* (e.g. Beuermann et al. 1999; Thomas et al. 1998). Their X-ray spectra are usually modelled as blackbodies, with  $kT \sim 20$  to 40 eV (e.g. Ramsay, Cropper & Mason 1996; Thomas & Beuermann 1998; Table 6.5 of Warner 1995). Although a harder component is often present, in most polars it only contributes a significant part of the flux in the *ROSAT* band during low states (Beuermann & Thomas 1993), where even very nearby polars are too faint to be included in the RBS (see also Section 6.2.2). A handful of confirmed and candidate polars that show no soft X-ray component, even in the high state, is now known (e.g. Ramsay & Cropper 2004, 2007; Ramsay et al. 2009; Vogel et al. 2008). However, these systems do not appear to be intrinsically very common. Only 2 are within 200 pc, and e.g. *XMM-Newton* and *INTEGRAL* and have not discovered many new polars (despite the nearest of the known hard polars, namely BY Cam, V1432 Aql, and V2301 Oph, being detected in the *INTEGRAL/IBIS* survey).

IPs have hard X-ray spectra, often modelled as intrinsically absorbed thermal bremsstrahlung with  $kT \sim 30$  keV (e.g. Patterson 1994; Frank, King & Raine 1985). In a few

IPs, a soft component is present (e.g. Haberl & Motch 1995; de Martino et al. 2004), but our sample does not contain any of these “soft IPs”. Depending on the accretion geometry, IPs can have very high intrinsic absorption (the intrinsic absorption also varies in individual systems). We take the intrinsic  $N_H$  as  $2 \times 10^{20} \text{ cm}^{-2}$  for EX Hya and DO Dra (Richman 1996; Mukai et al. 2003), and  $4 \times 10^{22} \text{ cm}^{-2}$  for CC Scl, AO Psc, TV Col, and EI UMa (Pietsch et al. 1987; Rana et al. 2004; Ramsay et al. 2008; Woudt et al. 2012), with a covering fraction of 0.5 in all cases.

We assume a  $kT = 30 \text{ eV}$  blackbody spectrum for the polars, and a  $kT = 30 \text{ keV}$  thermal bremsstrahlung spectrum for the IPs in our sample. These single temperature, single component spectra are not very physical (e.g. Norton & Watson 1989; Mukai et al. 2003; Beuermann, Burwitz & Reinsch 2012), and they are not expected to be good approximations for all sources in the sample. The assumed intrinsic absorption for the IPs in the sample are also rough approximations. Therefore, the values we give for  $L_X$  should be treated with caution. However, the space density estimate is much less sensitive to both the assumed X-ray spectra and the amount of intrinsic absorption we adopt for the IPs than are the estimated  $L_X$  values (we will return to this in Section 6.3.4).

Since this is a high Galactic Latitude sample, interstellar absorption is low for all our sources. A few systems are at sufficiently large distances that the total Galactic  $N_H$  (as given by Kalberla et al. 2005) is a good approximation. Many of the polars have  $N_H$  estimates from X-ray spectral fits (e.g. Schwope et al. 1997; Reinsch et al. 1994; Schwarz et al. 2009; Barrett, Singh & Mitchell 1999; Ramsay, Cropper & Mason 1996; Ramsay et al. 1994; Pandel & Córdova 2005; Schwope et al. 2007; Beuermann, Thomas & Pietsch 1991; Burwitz et al. 1998; Singh et al. 1995; Greiner, Schwarz & Wenzel 1998; Burwitz et al. 1997). For several systems, there are absorption measurements based on UV data (e.g. Araujo-Betancor et al. 2005; La Dous 1991; Verbunt 1987), and for a few more, Bruch & Engel (1994) give  $A_V$  estimates (we use the dust to gas ratio of Predehl & Schmitt 1995 to obtain  $N_H$ ). In cases where we have no observational estimate of interstellar absorption, we use the models of Amôres & Lépine (2005) and Drimmel et al. (2003).

We assume 50% errors in estimates of interstellar column densities, and give unabsorbed X-ray luminosities in the 0.12–2.48 keV band in Table 1.

## 6 CALCULATING THE SPACE DENSITY

### 6.1 The method

We describe the calculation that gives the space density, together with the uncertainty on that estimate only briefly. More detailed discussions may be found in Pretorius & Knigge (2012) and Pretorius et al. (2007b).

The effective observed volume of the RBS depends on the spacial distribution of CVs in the Galaxy, and on the X-ray luminosities of systems in the sample (since the survey is flux limited, rather than volume limited). It is found using the relation given by e.g. Stobie et al. (1989) and

Tinney et al. (1993):

$$V_j = \Omega \frac{h^3}{|\sin b|^3} [2 - (x_j^2 + 2x_j + 2) e^{-x_j}].$$

The index  $j$  represents mCVs in the sample;  $\Omega$  is the solid angle observed in the survey<sup>5</sup>, and  $x_j = d_j |\sin b|/h$ , with  $d_j$  the maximum distance at which system  $j$  could have been detected (a function of its luminosity, the flux limit, and extinction along all lines of sight covered by the survey). This relation assumes that  $\rho$  does not vary with radial position in the Galaxy, and that the vertical density profile is exponential. We assume scale-heights of  $h = 260 \text{ pc}$  for short-period systems, and  $h = 120 \text{ pc}$  for long-period systems<sup>6</sup>. To find  $d_j$ , we need  $N_H$  as a function of distance and  $b$ . For this we assume an exponential vertical density profile for gas, with a scale-height of 140 pc, and normalized to give  $N_H$  corresponding to  $A_V = 0.8 \text{ mag/kpc}$  in the Galactic Plane<sup>7</sup>.

The sum of the contributions of the 30 systems in the sample then gives the mid-Plane value of  $\rho$  ( $\rho_0 = \sum_j 1/V_j$ ). For the moment ignoring all errors, and simply assuming that the best-estimate distance, count rate, and  $N_H$  are the true values, we list the fractional contribution that each system in our sample makes to the total space density ( $\rho_j/\rho_0$ ) in the 8th column of Table 1. This shows that our  $\rho$  measurement is not dominated by 1 or 2 objects.

In order to correctly sample the full parameter space allowed by the data, and hence find the error on  $\rho_0$ , we compute its probability distribution function using a Monte Carlo simulation that calculates  $\rho_0$  for a large number of mock samples. The mock samples are created by drawing a distance,  $N_H$ , and count rate for every observed system from the appropriate distribution. These values are used to calculate each  $1/V_j$ , which is then weighted by a factor  $\mu_j$ , drawn from the probability distribution of the number of sources belonging to the population (corresponding to a particular observed system) that one expects to detect in the RBS (see Pretorius et al. 2007b and Pretorius & Knigge 2012).

### 6.2 Results

We have carried out this calculation for the whole observed sample of 30 mCVs, as well as for several sub-samples (polars, IPs, short- and long-period systems, and short-period polars and long-period IPs). Table 2 summarizes the results.

<sup>5</sup> Because  $b$  is variable over  $\Omega$ , we compute each  $V_j$  as a sum over smaller solid angles,  $\delta\Omega$ . The terms in this sum are slices subtended by  $2^\circ$  in  $b$ . These  $\delta\Omega$  are sufficiently small that the error introduced by  $b$  varying over  $\delta\Omega$  is negligible.

<sup>6</sup> The reason for this is that short- and long-period CVs are expected to be old and young populations, respectively. It is only a crude approximation, since systems can form at short period, and since polars at all periods are believed to evolve slowly. Our results do not change significantly if we simply assume the same  $h$  for all systems (see Section 6.3.2.)

<sup>7</sup> Since the survey covers a large area, at high galactic latitudes (all  $|b| > 30^\circ$ ), and the maximum distances we deal with are large compared to the typical size of inhomogeneities in the ISM, this smooth model for the density of gas is justified (for the most part, but see Section 6.2.2). We explore the sensitivity of our  $\rho$  estimate to the assumed mid-Plane gas density in Section 6.3.3.

**Table 2.** Space density estimates for all mCVs, IPs and polars separately, short- and long-period mCVs, and short-period polars and long-period IPs. UW Pic and J0859 + 05 are excluded from the samples split by  $P_{orb}$ , because their orbital periods fall in the period gap. In addition to the values inferred from the observed RBS sample, we list the estimates that would be obtained if polars are undercounted by a factor of 2, because of a high-state duty cycle of only 0.5.

Sample	$\rho_0/(10^{-7} \text{ pc}^{-3})$	
	No assumed low states	Polar duty cycle 0.5
All mCVs	$8.2^{+3.9}_{-2.3}$	$13^{+6.3}_{-3.8}$
Polars	$4.9^{+2.7}_{-1.5}$	$9.8^{+5.4}_{-3.1}$
IPs	$2.7^{+2.4}_{-1.2}$	
short- $P_{orb}$ mCVs	$4.6^{+3.2}_{-1.7}$	$8.3^{+5.7}_{-3.0}$
long- $P_{orb}$ mCVs	$2.8^{+1.8}_{-1.1}$	$3.8^{+3.2}_{-1.4}$
short- $P_{orb}$ polars	$3.6^{+2.5}_{-1.9}$	$7.2^{+5.0}_{-2.7}$
long- $P_{orb}$ IPs	$1.7^{+1.6}_{-0.9}$	

### 6.2.1 The probability distribution function of $\rho_0$

The distribution of  $\rho_0$  values, normalized to give a probability distribution function, from the simulation including all magnetic systems is shown in Fig. 2. The mode, median, and mean of the distribution are marked by solid lines at  $7.1 \times 10^{-7}$ ,  $8.2 \times 10^{-7}$ , and  $9.2 \times 10^{-7} \text{ pc}^{-3}$ , while the dashed lines at  $5.8 \times 10^{-7}$  and  $1.2 \times 10^{-6} \text{ pc}^{-3}$  show a 1- $\sigma$  confidence interval (the 16th and 84th percentile points of the distribution). In other words, our estimate for the mid-plane space density of mCVs is  $8.2^{+4}_{-2} \times 10^{-7} \text{ pc}^{-3}$ . We find that the large errors in many of the distances dominate the total uncertainty in  $\rho_0$ , although the small sample size and  $N_H$  errors also contribute significantly.

The inset in Fig. 2 shows the probability distribution functions of  $\rho_0$  for the whole mCV sample again, as well as for IPs (dotted histogram with lowest mode) and polars (dashed histogram) separately. We find space densities of  $3.2^{+2}_{-1} \times 10^{-7} \text{ pc}^{-3}$  for IPs and  $5.2^{+3}_{-2} \times 10^{-7} \text{ pc}^{-3}$  for polars.

### 6.2.2 Upper limits on the space density of an undetected population

The estimate above assumes that the detected population of mCVs is representative of the true underlying population, in the sense that it contains at least 1 of the faintest IPs and polars that occur in the intrinsic population (but not that it contains faint and bright systems in proportion to their intrinsic incidence; see Pretorius & Knigge 2012). Since the effective volume of the survey is smaller for fainter  $L_X$ , it is possible that even a large population of sources at the faint end of the luminosity function can go completely undetected. Here we place limits on the sizes of faint populations of polars and IPs that could escape detection in the RBS.

We again perform a Monte Carlo simulation with the same simple Galaxy model for stars and gas as described in Section 6.1 above (but, for simplicity, now assuming a single scale height of 260 pc for all mCVs). A model population of mCVs, all with the same  $L_X$ , and with a spectrum appropriate to either polars or IPs<sup>8</sup>, is distributed in the model

<sup>8</sup> For polars, we again assume a  $kT = 30 \text{ eV}$  blackbody spectrum,

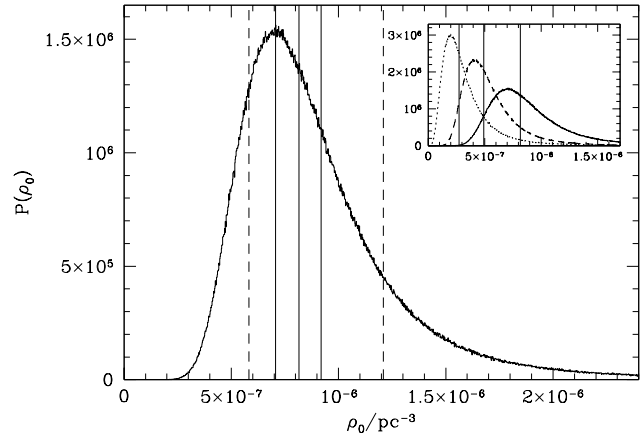


**Figure 2.** The  $\rho_0$  distribution for all mCVs, resulting from our simulation. Solid lines mark the mode, median, and mean at  $7.1 \times 10^{-7}$ ,  $8.2 \times 10^{-7}$ , and  $9.2 \times 10^{-7} \text{ pc}^{-3}$ . Dashed lines show a 1- $\sigma$  interval from  $5.8 \times 10^{-7}$  to  $1.2 \times 10^{-6} \text{ pc}^{-3}$ . The probability distribution functions shown in the inset are (with modes from high to low  $\rho_0$ ) for the whole mCV sample, polars alone (dashed), and IPs alone (dotted). In the inset, solid lines at  $8.2 \times 10^{-7}$ ,  $4.9 \times 10^{-7}$ , and  $2.7 \times 10^{-7} \text{ pc}^{-3}$  mark the medians of the three distributions.

Galaxy, in order to find the value of  $\rho_0$  for which the predicted number of detected systems is 3 (so that detecting 0 such systems is a 2- $\sigma$  result). We do this for a range of  $L_X$  below the faintest values found for the observed sample.

Fig. 3 shows the maximum allowed  $\rho_0$  as a function of  $L_X$ , separately for possible undetected polar and IP populations. The limits from the simulation are plotted as bold histograms, and the fine curves are fits to the data, given by

$$\rho_{max} = 1.02 \times 10^{-5} (L_X/10^{30} \text{ erg s}^{-1})^{-1.35} \text{ pc}^{-3}$$

for IPs, and

$$\rho_{max} = 4.01 \times 10^{-6} (L_X/10^{30} \text{ erg s}^{-1})^{-1.03} \text{ pc}^{-3}$$

for polars.  $\rho_{max}$  is only the upper limit on the mid-plane space density of an undetected population, and does not include the contribution from the observed systems. Thus, as a specific example, a population of undetected polars with a space density as high as  $5 \times$  the measured  $\rho_{polar}$  must have  $L_X \lesssim 10^{30} \text{ erg s}^{-1}$ . A hidden population of IPs can only have  $\rho_0 = 5 \times \rho_{IP}$  if it consists of systems with X-ray luminosities fainter than  $5 \times 10^{30} \text{ erg s}^{-1}$ .

Because the two relations given above involve  $L_X$ , which depends quite sensitively on our assumed X-ray spectra<sup>9</sup>, they are of only limited use (this is discussed further in Section 6.3.4).

This is also an instance where our smooth model of the ISM is not a valid approximation. This is because, e.g.,

and for IPs, we assume a  $kT = 30 \text{ keV}$  thermal bremsstrahlung spectrum with a partial covering absorber with covering fraction of 0.5 and  $N_H = 2 \times 10^{20} \text{ cm}^{-2}$ .

<sup>9</sup> For example, adopting blackbody temperatures of 10 and 50 eV for a moderately absorbed polar ( $N_H = 2 \times 10^{20} \text{ cm}^{-2}$ ), yield values of  $L_X$  that differ by a factor of 20. For the hard spectra of IPs,  $L_X$  is less sensitive to the assumed temperature of the bremsstrahlung spectrum, but does vary widely over an intrinsic  $N_H$  range as large as is observed.

polars with  $L_X = 10^{29}$  ergs $^{-1}$  can only be detected out to  $\simeq 40$  pc, which places them inside the ‘Local Bubble’ (e.g. Frisch, Redfield & Slavin 2011). However, since our model probably gives too high absorption at small distances, it only means that, at least for polars, the upper limit on  $\rho_0$  is conservative at the faint  $L_X$  end. In the case of IPs, the structure of the local ISM matters less, since their spectra are less affected by interstellar absorption.

Polars probably do not experience a large range in secular  $\dot{M}$  over the course of their evolution (because  $\dot{M}$  is a relatively flat function of  $P_{orb}$  when the only AML mechanism is GR). This means that we do not expect the polar luminosity function to rise towards the faint  $L_X$  end, beyond the luminosities that we are sensitive to. However, most (possibly all) polars switch between low- and high  $\dot{M}$  states on shorter timescales (e.g., Ramsay et al. 2004b). In the low photometric state, even very nearby polars are too faint to be included in the RBS. An example is AR UMa. It is at a distance of only 86 pc (Thorstensen, Lépine & Shara 2008), and is a bright soft X-ray source in its high state (e.g. Remillard et al. 1994), but was so faint during the RASS that it is not even included in the faint source catalogue. The deep low states of polars imply that in a single-epoch X-ray survey (which is what the RASS was over most of the sky) only a fraction of the local polar population that is equal to the high-state duty cycle can be detected. In other words, our assumption that the polar sample detected in the RBS is representative of the intrinsic population, is not strictly valid, since it does not include low-state systems. Ramsay et al. (2004b) find that polars spend roughly half their time in low states, implying that our estimate of  $\rho_{polar}$  is probably a factor of 2 too low<sup>10</sup>. In the final column of Table 2, we list the space density estimates that we obtain when allowing for a high-state duty cycle of 0.5 for polars and assuming that polars are undetectable their low states.

### 6.3 Sensitivity of the results to uncertain assumptions

Here we examine the sensitivity of our space density estimates to some of the more uncertain assumptions we made in calculating it. We will consider the possible impact of the systems with the most poorly constrained distances, the scale-heights we adopt for different CV populations, the assumed amount of interstellar absorption, the completeness of the sample at lower  $|b|$ , and the assumed X-ray spectra. By investigating an extreme range of assumptions, we show that possible systematic errors affect these space density estimates to less than roughly a factor of 2.

#### 6.3.1 The most uncertain distance estimates

Four members of the mCV sample, CV Hyi, FH UMa, IW Eri, and CD Ind, have very poorly constrained distances (see Section 4.2.3). The lower limits on distances are, however,

<sup>10</sup> Note that the high-state duty cycle of polars is not very well constrained; see e.g. Hessman, Gänsicke, & Mattei (2000), Araujo-Betancor et al. (2005), Wu & Kiss (2008), and Breedt et al. (2012).

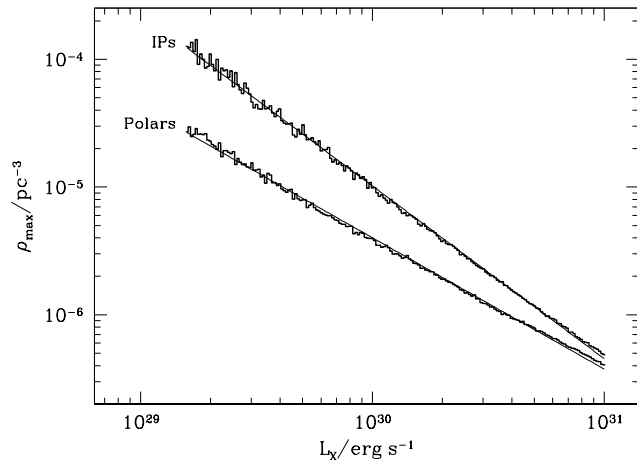


**Figure 3.** The upper limit on the mid-plane space density as a function of X-ray luminosity for an undetected population of polars and IPs. The data from the simulations are shown as a bold histogram, and fits are over-plotted as a finer lines. Note that the assumed X-ray spectra of polars and IPs are different, hence the different slopes.

always robust, and allow us to determine that these systems make at most a small contribution to the overall space density. Specifically, if we assume in each case the smallest allowed distance, the median of the  $\rho_0$  distribution would be at  $8.7 \times 10^{-7}$  pc $^{-3}$ , while neglecting the contributions of these 4 systems yield  $6.6 \times 10^{-7}$  pc $^{-3}$ . This is within the errors of our best estimate of  $8_{-2}^{+4} \times 10^{-7}$  pc $^{-3}$ . At its minimum allowed distance, IW Eri would account for 0.1 of the total space density, while the other 3 would all contribute less.

#### 6.3.2 The scale height of mCVs

We have assumed scale-heights of 260 and 120 pc for short- and long-period systems, respectively, as a crude approximation to the expectation that short- and long-period CVs belong to populations of different typical ages. If we instead set  $h$  to 260 or 120 pc for all systems, we obtain  $\rho_0$  distributions with medians at  $6.3 \times 10^{-7}$  pc $^{-3}$  and  $14 \times 10^{-7}$  pc $^{-3}$ , respectively. Therefore, although a plausible range of scale-heights shift the  $\rho_0$  distribution considerably, one would obtain estimates consistent with our result for other reasonable assumptions regarding the Galactic distribution of mCVs.

We have also checked that the  $z$ -distribution of the RBS mCV sample is consistent with the Galaxy model we use. In this calculation, we use the same model for the density of stars and gas, and assume the same X-ray spectra as before<sup>11</sup>. After imposing the RBS flux- and  $|b|$ -limits, we use a Kolmogorov-Smirnov (KS) test to compare model and observed  $z$ -distribution. We find that the whole sample of 30 observed systems, as well as subsamples consisting of short-

<sup>11</sup> Since the RBS is a high Galactic latitude, flux-limited survey, the observed sample does not have the same  $z$ -distribution as the underlying population. Generating a model  $z$ -distribution therefore involves an assumption regarding the luminosity function of the intrinsic polar and IP populations. We have assumed intrinsic distributions that are Gaussian in  $\log(L_X)$ , and experimented with several values for the average and standard deviation.

and long-period systems, have  $z$ -distributions that are consistent with both  $h = 260$  and  $120$  pc. In other words, our sample is too small, and the distance errors are too large, to distinguish between these two choices of scale height.

### 6.3.3 Interstellar absorption and completeness of the sample

Our treatment of interstellar absorption is very simple, and could be a concern, considering the soft, easily absorbed spectra of polars. As noted before, the unrealistically smooth model of the interstellar medium is not an important shortcoming (since we are using it to find a survey volume which covers a large fraction of the whole sky, at relatively high  $|b|$ , and since even the smaller maximum distances involved in the calculation are large enough to implying that we can average over regions of low and high absorption). The total amount of absorption, on the other hand, could have a large effect on the space density estimate, because higher absorption (along all lines of sight) reduces the survey volume.

We have set the mid-plane density of gas to produce  $A_V = 0.8$  mag/kpc for  $b = 0^\circ$ . A wide range in average mid-plane extinction has been reported. Drimmel et al. (2003) give  $A_V \simeq 0.7$  mag/kpc for lines of sight near the Galactic Plane in the inner disc of the Galaxy, and  $A_V \simeq 0.5$  mag/kpc in the outer Galactic disc. The model of Amôres & Lépine (2005) produces  $A_V \simeq 1$  mag/kpc, and Vergely et al. (1998) find  $1.2$  mag/kpc in the Galactic Plane. Repeating our space density calculation with the density of interstellar gas normalized to give values of  $0.5$  to  $1.2$  mag/kpc in the Plane, yields  $\rho_0$  distributions with median values of  $5.8 \times 10^{-7}$  and  $12 \times 10^{-7} \text{ pc}^{-3}$ , respectively<sup>12</sup>. This is consistent with our best estimate of  $8_{-2}^{+4} \times 10^{-7} \text{ pc}^{-3}$ .

We can also check for evidence that the completeness of our sample decreases at lower  $|b|$ , as one might expect from increasing absorption along lines of sight closer to the Galactic Plane. To do this we simply create subsamples with different  $|b|$  cutoffs. Compared to  $\rho = 8_{-2}^{+4} \times 10^{-7} \text{ pc}^{-3}$  from the whole sample of 30 systems ( $|b| > 30^\circ$ ), we find median  $\rho_0$  values of  $8.1 \times 10^{-7} \text{ pc}^{-3}$  and  $5.6 \times 10^{-7} \text{ pc}^{-3}$  for  $|b| > 40^\circ$  (17 systems) and  $|b| > 50^\circ$  (10 systems), respectively. These number are consistent to within the errors, and if there is a trend, it goes in the opposite direction than expected if the sample is less complete at lower  $|b|$ .

### 6.3.4 The assumed X-ray spectra

A final source of systematic uncertainty associated with the space density estimate is our assumed X-ray spectra. We have used simple, single component spectra for all systems (bremsstrahlung spectrum for IPs, and blackbodies polars). Here we will check the possible impact of a range of X-ray spectra on the space density estimates.

The space density calculation uses the maximum distance at which a given mCV in the observed sample could have been detected, since this determines the survey volume (for a population of systems with the same  $L_X$ ). For a given

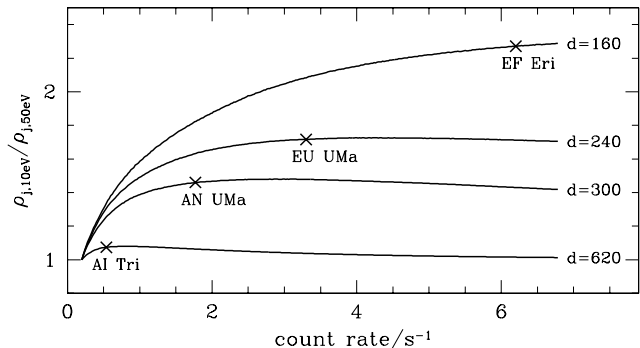


**Figure 4.** The ratio of the values of  $1/V_j$  obtained by assuming  $kT = 10$  and  $50$  eV blackbody spectra, as a function of the count rate at which the system is detected. The 4 curves are for different true distances. The count rates of 4 of the polars in our sample are indicated on the curves corresponding to their best-estimate distances. The largest effect of different spectra on  $\rho_j$  occurs for a system that lies at a small distance compared to the maximum distance it could have been detected at (since this implies a large amount of absorption between  $d$  and  $d_{max}$ ). The most extreme example in the RBS is EF Eri, where its contribution to the total space density would be a factor of about 2.2 larger for an assumed  $kT = 10$  eV than for an assumed  $kT = 50$  eV spectrum.

object, the maximum distance depends on the ratio of  $F_X$  to the flux limit, which may as well be expressed as a ratio of observed count rate to limiting count rate. This means that the assumed X-ray spectral shape has relatively little influence on the space density calculation (only the interstellar absorption depends on the X-ray spectrum, and this only matters to the extent that  $N_H$  differs between the true and maximum distance, and that the slope of absorption as a function of  $N_H$  differs for different spectra).

To show this more explicitly, if  $y$  is the ratio of count rate ( $c$ ) to X-ray flux (i.e.  $y = c/F_X$ , a function of the spectrum, the instrument response, and  $N_H$ ), then the distance is  $d = \sqrt{yL_X/4\pi c}$ , so  $d_{max} = \sqrt{y_{max}c/y_{lim}}$ , where  $y_{max} = y(d_{max})$  and  $c_{lim}$  is the limiting count rate. Then, for  $d \simeq d_{max}$  (the case of a system detected at close to the limiting count rate), and for large  $d$  ( $N_H$  at  $d$  already at about the total value for the Galaxy),  $y_{max} \simeq y$ , implying that the shape of  $y(N_H)$  does not matter, and different spectra give the same  $d_{max}$  (and therefore  $1/V_{max}$ ). Otherwise, the difference in  $d_{max}$  resulting from assuming different spectra depends on the difference in slope of  $y(N_H)$  for those spectra. We illustrate this in Fig. 4, where we use blackbody spectra with  $kT = 10$  and  $50$  eV. The figure shows that, while different assumed spectra imply very different values of  $L_X$ , the space density contribution of a given system changes by at most a factor of  $\simeq 2$ , with a much smaller effect in most cases. The effect is also smaller for spectra appropriate to IPs than for the soft spectra of polars.

For the whole sample of polars, we would obtain median  $\rho_0$  values of  $8.1 \times 10^{-7} \text{ pc}^{-3}$  and  $4.5 \times 10^{-7} \text{ pc}^{-3}$  assuming a  $kT = 10$  and  $50$  eV blackbody spectrum, respectively, compared to  $\rho_{polar} = 5_{-2}^{+3} \times 10^{-7} \text{ pc}^{-3}$  for our favoured  $30$  eV spectrum. Note that while a  $kT = 30$  eV blackbody spectrum is unlikely to be a good approximation for all the polars in our sample, we also do not expect all to be better represented by either much lower or much higher temperature blackbodies.

<sup>12</sup>  $\rho_{IP}$  on its own is much less sensitive to this, because of the harder spectra of IPs, and because intrinsic absorption reduces the importance of interstellar absorption.

$\rho_{IP}$  is less sensitive to the assumed spectrum, because the difference in absorption between different hard, intrinsically absorbed spectra is small, even for a large range in assumed temperature. Our best model is a  $kT = 30$  keV thermal bremsstrahlung spectrum, with intrinsic column densities of  $2 \times 10^{20} \text{ cm}^{-2}$  for EX Hya and DO Dra, and  $4 \times 10^{22} \text{ cm}^{-2}$  for CC Scl, AO Psc, TV Col, and EI UMa, all with a covering fraction of 0.5. We will separately consider different bremsstrahlung temperatures and intrinsic absorption. With  $kT = 10$  and  $50$  keV, respectively, we obtain median  $\rho_0$  values of  $2.8 \times 10^{-7} \text{ pc}^{-3}$  and  $2.6 \times 10^{-7} \text{ pc}^{-3}$  for the sample of 6 IPs, compared to our best estimate of  $3_{-1}^{+2} \times 10^{-7} \text{ pc}^{-3}$ . Assuming  $kT = 30$  keV for IPs, but with either high ( $N_H = 4 \times 10^{22} \text{ cm}^{-2}$  and a covering fraction of 1 for all systems) or no intrinsic absorption, we find  $\rho_0$  distributions with medians at  $2.5 \times 10^{-7} \text{ pc}^{-3}$  and  $2.8 \times 10^{-7} \text{ pc}^{-3}$ , respectively.

The upper limits on the space densities of hypothetical hidden populations of IPs and polars are of course also affected by the assumed X-ray spectrum. Since we find the upper limits as a function of the X-ray luminosity of the undetected population (and  $L_X$ , for the detected as well as “hidden” systems, depends on the assumed X-ray spectrum), we present the effect of assuming different X-ray spectra as the ratio of  $\rho_{max}$  and the best-estimate measured  $\rho_0$ , as a function of the ratio of  $L_X$  of the hidden population and the faintest detected system. In other words, we fix  $\rho_{polar} = 5 \times 10^{-7} \text{ pc}^{-3}$  and  $\rho_{IP} = 3 \times 10^{-7} \text{ pc}^{-3}$ , and then find  $\rho_{max,polar}$  and  $\rho_{max,IP}$ , as well as  $L_X$  of the hidden population of IPs and polars and of our faintest observed IP and polar with different assumed spectra. The result is shown in Fig. 5. In the case of polars, a population with a space density as high as  $5 \times$  the measured  $\rho_{polar}$  (i.e.,  $\rho_{max} \simeq 4 \times 10^{-6} \text{ pc}^{-3}$  must have  $L_X \lesssim 0.06 \times$  the luminosity of EQ Cet, the faintest polar in the RBS sample. An undetected IP population must have  $L_X \lesssim 0.2 \times$  the luminosity of the faintest detected system (CC Scl) in order for its space density to be as high as  $5 \times \rho_{IP}$  (i.e.,  $\rho_{max} \simeq 1.4 \times 10^{-6} \text{ pc}^{-3}$ ). These ratios are not very sensitive to the spectrum we assume (see the size of the hatched areas in Fig. 5).

## 7 DISCUSSION

Having derived space density estimates for polars and IPs, let us revisit the three key questions that provided the main motivation for our study (see Sections 1 and 2). We note from the outset that our goal here is merely to take a brief look at some of the implications of our results; a full analysis of these issues is well beyond the scope of the present paper.

### 7.1 The relationship between intermediate polars and polars

As noted in Section 2, a natural explanation for the lack of short- $P_{orb}$  IPs is that long-period IPs evolve into polars below the period gap. If one assumes that long-period IPs are the sole progenitors of short-period polars, and that all IPs synchronize once they have crossed the period gap, then the ratio of the space densities of long- $P_{orb}$  IPs and short- $P_{orb}$

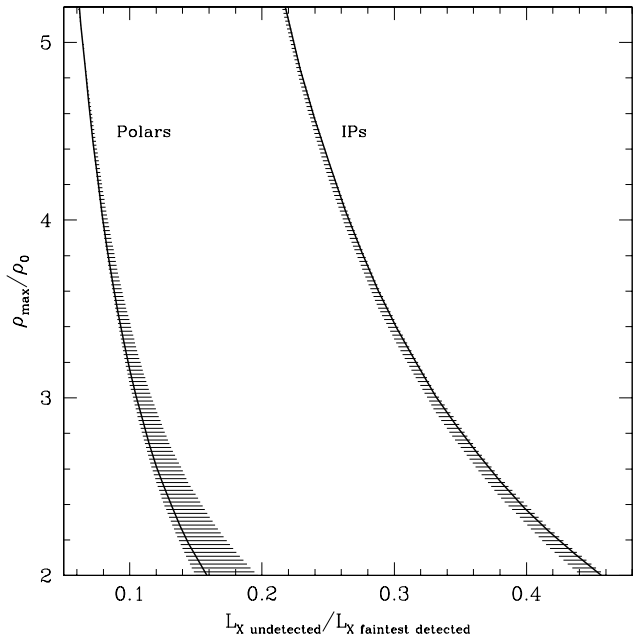


**Figure 5.**  $\rho_{max,IP}/\rho_{IP}$  and  $\rho_{max,polar}/\rho_{polar}$  as a function of the ratios of the luminosity of a hidden population and the luminosity of the faintest detected IP/polar (CC Scl/EQ Cet). The bold curves are for our best model (a 30 eV blackbody spectrum for polars and partially absorbed 30 keV thermal bremsstrahlung spectra for IPs). The hatched areas show the sensitivity to the assumed spectra. For polars, this corresponds to the area between the curves obtained by assuming respectively  $kT = 10$  and  $50$  eV blackbody spectra in calculating  $\rho_{max,polar}$  and X-ray luminosities for both the undetected population and EQ Cet (while  $\rho_{polar}$  is fixed at  $5 \times 10^{-7} \text{ pc}^{-3}$ ). For IPs, the hatched area corresponds to  $kT = 10$  and  $50$  keV bremsstrahlung spectra.

polars ( $\rho_{IP,lp}$  and  $\rho_{polar,sp}$ ) should simply reflect their relative evolutionary time-scales. For the purpose of our qualitative discussion, let us throw caution to the wind and assume that the numbers in Table 2 are reasonable approximations to the total space densities, even though our samples are flux-limited and even though polars and IPs have quite different X-ray luminosity functions.

We then find that the observed logarithm of this ratio is  $\log(\rho_{polar,sp}/\rho_{IP,lp}) = 0.32 \pm 0.36$  (this becomes  $\log(\rho_{polar,sp}/\rho_{IP,lp}) = 0.63 \pm 0.36$ , if we assume a 0.5 high-state duty cycle for polars). The ratio itself is therefore  $\simeq 2$ , but this is accurate to only about a factor of two. If the evolution of long-period IPs is really driven by MB, while that of short-period polars is driven solely by GR, the evolutionary time-scale of the latter is expected to exceed that of the former by at least a factor of  $\gtrsim 5$  (e.g. Knigge et al. 2011). This is larger than the ratio of the inferred space densities, but still completely consistent with it, given the rather large statistical errors. In fact, at  $2\text{-}\sigma$ , the uncertainties are large enough to encompass both ratios exceeding 10 and ratios less than unity. This means that, with the currently available space density estimates for polars and IPs, we cannot place strong constraints on the evolutionary relationship between the two classes. Nevertheless, it is interesting to note that the simplest possible model, in which short-period polars derive from long-period IPs, is not ruled out by their observed space densities.

## 7.2 The intrinsic fraction of magnetic CVs

We can also combine our measurement of the space density of mCVs (polars as well as IPs) with that of non-magnetic CVs (Pretorius & Knigge 2012; Pretorius et al. 2007b) in order to obtain an estimate of the intrinsic fraction of mCVs amongst the Galactic CV population ( $f_{mCV}$ ). This again involves throwing caution to the wind to some extent, since the samples involved are flux-limited, and the populations being compared have different X-ray luminosity functions. Thus it is quite possible that our estimate of the mCV fraction is still affected by selection biases.

Keeping this caveat in mind, we find that  $\log(f_{mCV}) = -0.80^{+0.27}_{-0.36}$ , i.e.  $f_{mCV} \simeq 16\%$ , to within a factor of 2 (or  $\log(f_{mCV}) = -0.63^{+0.24}_{-0.33}$ , if half of all polars are in the low state at a given time, and thus undetected in the RBS). This is consistent with the raw incidence of mCVs in the known CV sample ( $\simeq 20\%$ ; see Ritter & Kolb 2003). However, more importantly, it is also consistent, within our considerable uncertainties, with the fraction of isolated WDs that are strongly magnetic ( $\sim 10\%$ ). In fact, it seems likely that our X-ray-selected CV sample is more complete for mCVs than it is for non-magnetic CVs. If so, our estimate of  $f_{mCV}$  should be considered as an upper limit. Thus the incidence of magnetism is not obviously enhanced amongst CV primaries compared to isolated WDs.

## 7.3 Galactic X-ray Source Populations

As noted in Section 2, mCVs – and particularly IPs – have been suggested to be the dominant X-ray source populations above  $L_X \simeq 10^{31} \text{ergs}^{-1}$  in a variety of Galactic environments. We can use our new space density estimates to check whether mCVs can plausibly account for the number of sources seen in surveys of these environments.

Let us take the Galactic Centre region as an example. The deep Chandra survey of Muno et al. (2009) covers an effective area of  $\simeq 10^{-3} \text{deg}^2$  down to  $L_X \simeq 10^{31} \text{ergs}^{-1}$  and includes  $\simeq 9000$  sources. For our order of magnitude estimate here, we will ignore subtleties like the flux/luminosity-dependent survey area and simply ask if it is plausible that the majority of these sources may be IPs.

Given that the stellar density distribution is highly peaked towards the Galactic Centre, let us approximate the volume covered by the survey as a sphere of radius  $R \simeq 150 \text{pc}$ . The space density of X-ray sources in the Galactic Centre is then of order  $\rho_{X,GC} \sim 6 \times 10^{-4} \text{pc}^{-3}$ , while the local space density of IPs is  $\rho_{IP} \sim 3 \times 10^{-7} \text{pc}^{-3}$ . However, the stellar space density in the Galactic centre is  $\simeq 70 \text{pc}^{-3}$ , while it is only  $\simeq 0.044 \text{pc}^{-3}$  in the solar neighborhood (e.g. Hong et al. 2009). We thus find that there is roughly 1 X-ray source per 100,000 stars in the Galactic centre, and roughly 1 IP per 200,000 stars in the solar neighborhood. At the level of precision to which we are working here, these numbers are identical. We thus conclude that IPs remain a viable explanation for most of the X-ray sources seen in the Galactic Centre.

It should be obvious that the calculation above is not to be taken too seriously. Its purpose is merely to illustrate how our measurement of the space density of mCVs, in general, and IPs, in particular, relates to recent X-ray surveys in a wide variety of Galactic environments. A correct analysis

would have to account in much more detail for the properties of the various surveys. This is worth doing, but beyond the scope of the present paper.

## 7.4 Outlook

The rough calculations above show that open questions concerning the evolution and Galactic abundance of mCVs cannot yet be conclusively answered. This highlights a fundamental problem: given the limited size of the existing flux-limited CV samples, and the low precision of most available distance estimates, it is currently impossible to measure space densities to an accuracy much better than a factor of  $\simeq 2$ . To make matters worse, we often need ratios of space densities for various sub-populations in order to test evolutionary models, which necessarily suffer from even lower precision.

This situation should improve dramatically over the coming years. Surveys with *eROSITA* will reach flux limits around 2 orders of magnitude deeper than the RBS and will yield large X-ray-selected mCV samples (e.g. Schwöpe 2012), while *Gaia* will provide accurate distance measurements for a large number of CVs.

## 8 CONCLUSIONS

We have used a complete, purely X-ray flux-limited sample of 30 mCVs from the RBS to place constraints on the local space density of these systems. Our conclusions are listed below.

(i) Assuming that the sample used here is representative of the intrinsic population (in the sense that the RBS detected at least one IP and one polar at the faintest ends of the luminosity functions of those populations), we obtain a mid-plane space density of  $8_{-2}^{+4} \times 10^{-7} \text{pc}^{-3}$  for mCVs. For the two distinct types of mCVs, we find  $\rho_{polar} = 5_{-2}^{+3} \times 10^{-7} \text{pc}^{-3}$  and  $\rho_{IP} = 3_{-1}^{+2} \times 10^{-7} \text{pc}^{-3}$ . If we assume that polars are detectable in X-rays for only 50% of the time, we obtain  $\rho_{polar} = 1_{-0.3}^{+0.5} \times 10^{-6} \text{pc}^{-3}$  and  $\rho_{mCV} = 1.3_{-0.6}^{+0.6} \times 10^{-6} \text{pc}^{-3}$ .

(ii) We have calculated the maximum sizes of hypothetical faint populations of IPs and polars that are consistent with their non-detection in the RBS, as a function of the X-ray luminosity of the undetected populations. If an undetected population of polars with a space density  $5\times$  as high as the space density we infer from detected systems exists, then those systems must have  $L_X \lesssim 0.06\times$  the luminosity of the faintest polar in the RBS sample (EQ Cet). In the case of IPs, an undetected population with  $L_X \lesssim 0.2\times$  the luminosity of the faintest detected system (CC Scl) can have a space density as high as  $5\times$  the value we measure from the detected IPs.

(iii) The ratio of the space density of short-period polars to long-period IPs is  $2_{-1}^{+3}$  (or  $4_{-2}^{+6}$ , assuming a 50% high-state duty cycle for polars). Within the large errors, this is consistent with the very simple hypothesis that (the majority of) long-period IPs evolve into short-period polars, and that this accounts for the whole population of short-period polars.

(iv) Our estimate of the intrinsic fraction of mCVs is consistent with the fraction of magnetic systems in the known CV sample ( $\simeq 0.2$ ). However, with existing data, this fraction cannot be measured to high enough precision to rule out an incidence of mCVs as low as  $\simeq 10\%$ . It is therefore not clear whether the fraction of strongly magnetic WDs is higher in CVs than in the single WD population.

(v) When the local space density of IPs is scaled to the density of stars in the Galactic Centre, it is sufficiently high to account for the number of bright ( $L_X \gtrsim 10^{31}$  ergs $^{-1}$ ) X-ray sources detected in that region.

## ACKNOWLEDGEMENTS

We thank Kars Verbeek for taking snapshot IR images of V4738 Sgr and RS Cae.

## REFERENCES

- Ak T., Bilir S., Ak S., Eker Z., 2008, *NewA*, 13, 133
- Amôres E. B., Lépine J. R. D., 2005, *AJ*, 130, 659
- Araujo-Betancor S., Gänsicke B.T., Long K.S., Beuermann K., de Martino D., Sion E.M., Szkody P., 2005, *ApJ*, 622, 589
- Bailey J., 1981, *MNRAS*, 197, 31
- Barrett P., Singh K. P., Mitchell S., in Hellier C., Mukai K., eds, ASP Conf. Ser. Vol. 157, Annapolis Workshop on Magnetic Cataclysmic Variables. Astron. Soc. Pac., San Francisco, p. 180
- Beuermann, K. 2000, *NewAR*, 44, 93
- Beuermann K., Burwitz V., 1995, *ASPC*, 85, 99
- Beuermann K., Schwope A. D., 1994, in Shafter A. W., ed., ASP Conf. Ser. Vol. 56, Interacting Binary Stars. Astron. Soc. Pac., San Francisco p. 119
- Beuermann K., Thomas H.-C., 1993, *AdSpR*, 13, 115
- Beuermann K., Burwitz V., Reinsch K., 2012, *A&A*, 543, A41
- Beuermann K., Thomas H.-C., Pietsch W., 1991, *A&A*, 246, L36
- Beuermann K., Schwope A., Weissieker H., Motch C., 1985, *SSRv*, 40, 135
- Beuermann K., Thomas H.-C., Reinsch K., Schwope A. D., Trümper J., Voges W., 1999, *A&A*, 347, 47
- Beuermann K., Harrison T. E., McArthur B. E., Benedict G. F., Gänsicke B. T., 2003, *A&A*, 412, 821
- Beuermann, K., Diese, J., Paik, S., Ploch, A., Zachmann, J., Schwope, A. D., & Hessman, F. V. 2009, *A&A*, 507, 385
- Bonnet-Bidaud, J. M., Mouchet, M., Somova, T. A., & Somov, N. N. 1996, *A&A*, 306, 199
- Breedt E., Gänsicke B. T., Girven J., Drake A. J., Copperwheat C. M., Parsons S. G., Marsh T. R., 2012, *MNRAS*, 423, 1437
- Brinkworth C. S., et al., 2007, *ApJ*, 659, 1541
- Bruch A., Engel A., 1994, *A&AS*, 104, 79
- Burwitz V., Reinsch K., Schwope A. D., Beuermann K., Thomas H.-C., Greiner J., 1996, *A&A*, 305, 507
- Burwitz V., Reinsch K., Beuermann K., Thomas H.-C., 1997, *A&A*, 327, 183
- Burwitz V., et al., 1998, *A&A*, 331, 262
- Butters O. W., Katajainen S., Norton A. J., Lehto H. J., Pirola V., 2009, *A&A*, 496, 891
- Cao L., Wei J.-Y., Hu J.-Y., 1999, *A&AS*, 135, 243
- Chanmugam G., Ray A., 1984, *ApJ*, 285, 252
- Chen A., O'Donoghue D., Stobie R. S., Kilkenny D., Warner B., 2001, *MNRAS*, 325, 89
- Ciardi, D. R., Howell, S. B., Hauschildt, P. H., & Allard, F. 1998, *ApJ*, 504, 450
- Clayton, K. L., & Osborne, J. P. 1994, *MNRAS*, 268, 229
- Cropper M., 1990, *SSRv*, 54, 195
- Cumming A., 2002, *MNRAS*, 333, 589
- de Martino D., Matt G., Belloni T., Haberl F., Mukai K., 2004, *A&A*, 415, 1009
- Drimmel R., Cabrera-Lavers A., López-Corredoira M., 2003, *A&A*, 409, 205
- Frank J., King A. R., Raine D. J., 1985, *Accretion Power in Astrophysics*, Cambridge Univ. Press, Cambridge
- Frisch P. C., Redfield S., Slavin J. D., 2011, *ARA&A*, 49, 237
- Gänsicke B. T., 1999, in Hellier C., Mukai K., eds, ASP Conf. Ser. 157, Proc. Annapolis Workshop on Magnetic Cataclysmic Variables. Astron. Soc. Pac., San Francisco, p. 261
- Gänsicke B. T., et al., 2009, *MNRAS*, 397, 2170
- Gioia I.M., Henry J.P., Mullis C.R., Böhringer H., Briel U.G., Voges W., Huchra J.P., 2003, *ApJS*, 149, 29
- Glass I. S., Nagata T., 2000, *MNSSA*, 59, 110
- Glenn J., Howell S. B., Schmidt G. D., Liebert J., Grauer A. D., Wagner R. M., 1994, *ApJ*, 424, 967
- Greiner J., Schwarz R., Wenzel W., 1998, *MNRAS*, 296, 437
- Haberl, F., & Motch, C. 1995, *A&A*, 297, L37
- Heinke C. O., Grindlay J. E., Edmonds P. D., Cohn H. N., Luggner P. M., Camilo F., Bogdanov S., Freire P. C., 2005, *ApJ*, 625, 796
- Hellier C., 1993, *MNRAS*, 264, 132
- Henry J.P., Mullis C.R., Voges W., Böhringer H., Briel U.G., Gioia I.M., Huchra J.P., 2006, *ApJS*, 162, 304
- Hessman F. V., Gänsicke B. T., Mattei J. A., 2000, *A&A*, 361, 952
- Hoard D. W., Linnell A. P., Szkody P., Sion E. M., 2005, *AJ*, 130, 214
- Hong J. S., van den Berg M., Grindlay J. E., Laycock S., 2009, *ApJ*, 706, 223
- Hong J., van den Berg M., Grindlay J. E., Servillat M., Zhao P., 2012, *ApJ*, 746, 165
- Howell S. B., Sirk M. M., Malina R. F., Mittaz J. P. D., Mason K. O., 1995, *ApJ*, 439, 991
- Kalberla P. M. W., Burton W. B., Hartmann D., Arnal E. M., Bajaja E., Morras R., Pöppel W. G. L., 2005, *A&A*, 440, 775
- Katajainen S., Lehto H. J., Pirola V., Karttunen H., Piironen J., 2000, *A&A*, 357, 677
- Kawka A., Vennes S., Schmidt G. D., Wickramasinghe D. T., Koch R., 2007, *ApJ*, 654, 499
- King A. R., Frank J., Ritter H., 1985, *MNRAS*, 213, 181
- Knigge C., 2006, *MNRAS*, 373, 484
- Knigge C., Baraffe I., Patterson J., 2011, *ApJS*, 194, 28
- Krivonos R., Revnivtsev M., Churazov E., Sazonov S., Grebenev S., Sunyaev R., 2007, *A&A*, 463, 957
- Krzeminski W., Serkowski K., 1977, *ApJ*, 216, L45
- Külebi B., Jordan S., Euchner F., Gänsicke B. T., Hirsch

- H., 2009, *A&A*, 506, 1341
- La Dous C., 1991, *A&A*, 252, 100
- Lamb D. Q., Melia F., 1987, *Ap&SS*, 131, 511
- Li J., Wickramasinghe D. T., 1998, *MNRAS*, 300, 718
- Liebert J., Tapia S., Bond H. E., Grauer A. D., 1982, *ApJ*, 254, 232
- Lutz T. E., Kelker D. H., 1973, *PASP*, 85, 573
- Malmquist, K.G. 1924, *Medd. Lund Astron. Obs.*, 2(32), 64
- Mateo M., Szkody P., Garnavich P., 1991, *ApJ*, 370, 370
- McArthur B. E., et al., 2001, *ApJ*, 560, 907
- Mittaz J. P. D., Rosen S. R., Mason K. O., Howell S. B., 1992, *MNRAS*, 258, 277
- Monet D. G., et al., 2003, *AJ*, 125, 984
- Morris S. L., Schmidt G. D., Liebert J., Stocke J., Gioia I. M., Maccacaro T., 1987, *ApJ*, 314, 641
- Mouchet M., Bonnet-Bidaud J. M., Buckley D. A. H., Tuohy I. R., 1991, *A&A*, 250, 99
- Mukai K., Kinkhabwala A., Peterson J. R., Kahn S. M., Paerels F., 2003, *ApJ*, 586, L77
- Muno M. P., et al., 2004, *ApJ*, 613, 1179
- Muno M. P., Bauer F. E., Bandyopadhyay R. M., Wang Q. D., 2006, *ApJS*, 165, 173
- Muno M. P., et al., 2009, *ApJS*, 181, 110
- Nagayama T., et al., 2003, *SPIE*, 4841, 459
- Norton, A. J., & Watson, M. G. 1989, *MNRAS*, 237, 853
- Norton A. J., Wynn G. A., Somerscales R. V., 2004, *ApJ*, 614, 349
- Norton A. J., Beardmore A. P., Retter A., Buckley D. A. H., 2000, *MNRAS*, 312, 362
- Osborne J. P., Beardmore A. P., Wheatley P. J., Hakala P., Watson M. G., Mason K. O., Hassall B. J. M., King A. R., 1994, *MNRAS*, 270, 650
- Pandel D., Córdova F. A., 2005, *ApJ*, 620, 416
- Patterson J., 1984, *ApJS*, 54, 443
- Patterson J., 1994, *PASP*, 106, 209
- Patterson J., 2011, *MNRAS*, 411, 2695
- Patterson J., Moulden M., 1993, *PASP*, 105, 779
- Patterson J., Price C. M., 1981, *ApJ*, 243, L83
- Patterson J., et al., 2005, *PASP*, 117, 1204
- Peters C. S., 2008, PhD thesis, Dartmouth College
- Pietsch W., Voges W., Kendziorra E., Pakull M., 1987, *Ap&SS*, 130, 281
- Predehl P., Schmitt J.H.M.M., 1995, *A&A*, 293, 889
- Pretorius M. L., Knigge C., 2012, *MNRAS*, 419, 1442
- Pretorius M. L., Knigge C., Kolb U., 2007a, *MNRAS*, 374, 1495
- Pretorius M. L., Knigge C., O'Donoghue D., Henry J. P., Gioia I. M., Mullis C. R., 2007b, *MNRAS*, 382, 1279
- Ramsay G., Cropper M., 2004, *MNRAS*, 347, 497
- Ramsay G., Cropper M., 2007, *MNRAS*, 379, 1209
- Ramsay G., Cropper M., Mason K. O., 1996, *MNRAS*, 278, 285
- Ramsay G., Mason K. O., Cropper M., Watson M. G., Clayton K. L., 1994, *MNRAS*, 270, 692
- Ramsay G., Buckley D. A. H., Cropper M., Harrop-Allin M. K., 1999, *MNRAS*, 303, 96
- Ramsay, G., Cropper, M., Mason, K. O., Córdova, F. A., & Priedhorsky, W. 2004a, *MNRAS*, 347, 95
- Ramsay G., Cropper M., Wu K., Mason K. O., Córdova F. A., Priedhorsky W., 2004b, *MNRAS*, 350, 1373
- Ramsay G., Wheatley P. J., Norton A. J., Hakala P., Baskill D., 2008, *MNRAS*, 387, 1157
- Ramsay G., Rosen S., Hakala P., Barclay T., 2009, *MNRAS*, 395, 416
- Rana, V. R., Singh, K. P., Schlegel, E. M., & Barrett, P. 2004, *AJ*, 127, 489
- Reimer T. W., Welsh W. F., Mukai K., Ringwald F. A., 2008, *ApJ*, 678, 376
- Reinsch K., Burwitz V., Beuermann K., Schwöpe A. D., Thomas H.-C., 1994, *A&A*, 291, L27
- Remillard, R. A., Schachter, J. F., Silber, A. D., Slane, P. 1994, *ApJ*, 426, 288
- Revnivtsev M., Sazonov S., Gilfanov M., Churazov E., Sunyaev R., 2006, *A&A*, 452, 169
- Revnivtsev M., Sazonov S., Krivonos R., Ritter H., Sunyaev R., 2008, *A&A*, 489, 1121
- Richman H. R., 1996, *ApJ*, 462, 404
- Ritter H., Kolb U., 2003, *A&A*, 404, 301 (update *RK-cat7.18*, 2012)
- Rodrigues, C. V., Jablonski, F. J., D'Amico, F., Cieslinski, D., Steiner, J. E., Diaz, M. P., Hickel, G. R. 2006, *MNRAS*, 369, 1972
- Romero-Colmenero E., Potter S. B., Buckley D. A. H., Barrett P. E., Vrielmann S., 2003, *MNRAS*, 339, 685
- Sazonov S., Revnivtsev M., Gilfanov M., Churazov E., Sunyaev R., 2006, *A&A*, 450, 117
- Schmidt G. D., Szkody P., Smith P. S., Silber A., Tovmassian G., Hoard D. W., Gänsicke B. T., de Martino D., 1996, *ApJ*, 473, 483
- Schmidt G. D., Ferrario L., Wickramasinghe D. T., Smith P. S., 2001, *ApJ*, 553, 823
- Schwarz R., et al., 1998, *A&A*, 338, 465
- Schwarz R., Schwöpe A. D., Vogel J., Dhillon V. S., Marsh T. R., Copperwheat C., Littlefair S. P., Kanbach G., 2009, *A&A*, 496, 833
- Schwöpe A., 2012, in Giovanelli F., Sabau-Graziati L., eds, *The golden age of cataclysmic variables and related objects*, *Mem. S. A. It. Vol. 83*, p. 844
- Schwöpe A. D., Schreiber M. R., Szkody P., 2006, *A&A*, 452, 955
- Schwöpe A. D., Schwarz R., Greiner J., 1999, *A&A*, 348, 861
- Schwöpe A. D., Thomas H. C., Beuermann K., 1993, *A&A*, 271, L25
- Schwöpe A. D., Buckley D. A. H., O'Donoghue D., Hasinger G., Truemper J., Voges W., 1997, *A&A*, 326, 195
- Schwöpe A., et al., 2000, *AN*, 321, 1
- Schwöpe A.D., Brunner H., Buckley D., Greiner J., Heyden K.v.d., Neizvestny S., Potter S., Schwarz R., 2002, *A&A*, 396, 895
- Schwöpe A. D., Staude A., Koester D., Vogel J., 2007, *A&A*, 469, 1027
- Singh K. P., et al., 1995, *ApJ*, 453, L95
- Skrutskie M.F., et al., 2006, *AJ*, 131, 1163
- Sproats L. N., Howell S. B., Mason K. O., 1996, *MNRAS*, 282, 1211
- Sterken C., Vogt N., Freeth R., Kennedy H. D., Page A. A., Marino B. F., Walker W. S. G., 1983, *A&A*, 118, 325
- Stobie R. S., Ishida K., Peacock J. A., 1989, *MNRAS*, 238, 709
- Tappert C., Augusteijn T., Maza J., 2004, *MNRAS*, 354, 321

- Thomas H.-C., Beuermann K., 1998, in Breitschwerdt D., Freyberg M.J., Truemper J., eds, *Lecture Notes in Physics* Vol. 506, *The Local Bubble and Beyond*. Springer-Verlag, Berlin, p. 247
- Thomas H.-C., Beuermann K., Schwope A. D., Burwitz V., 1996, *A&A*, 313, 833
- Thomas H.-C., Beuermann K., Reinsch K., Schwope A. D., Truemper J., Voges W., 1998, *A&A*, 335, 467
- Thorstensen, J. R. 1986, *AJ*, 91, 940
- Thorstensen J. R., 2003, *AJ*, 126, 3017
- Thorstensen J. R., Lépine S., Shara M., 2008, *AJ*, 136, 2107
- Thorstensen J. R., Schwarz R., Schwope A. D., Staude A., Vogel J., Krumpe M., Kohnert J., Nebot Gómez-Morán A., 2009, *PASP*, 121, 465
- Tinney C. G., Reid I. N., Mould J. R., 1993, *ApJ*, 414, 254
- Tout C. A., Wickramasinghe D. T., Liebert J., Ferrario L., Pringle J. E., 2008, *MNRAS*, 387, 897
- Townsley D. M., Gänsicke B. T., 2009, *ApJ*, 693, 1007
- Verbunt F., 1987, *A&AS*, 71, 339
- Vergely J.-L., Ferrero R. F., Egret D., Koeppen J., 1998, *A&A*, 340, 543
- Visvanathan N., Bessell M. S., Wickramasinghe D. T., 1984, *IAUC*, 3923, 2
- Vogel J., Byckling K., Schwope A., Osborne J. P., Schwarz R., Watson M. G., 2008, *A&A*, 485, 787
- Voges W., et al., 1999, *A&A*, 349, 389
- Voges W., et al., 2000, *IAUC*, 7432, 3
- Warner B., 1995, *Cataclysmic Variable Stars*. Cambridge Univ. Press, Cambridge
- Wickramasinghe D. T., Wu K., Ferrario L., 1991, *MNRAS*, 249, 460
- Williams, G., Johns, M., Price, C., Hiltner, A., Boley, F., Maker, S., & Mook, D. 1979, *Nature*, 281, 48
- Woudt P. A., et al., 2012, *MNRAS*, in press (arXiv:1208.5936)
- Wright E. L., et al., 2010, *AJ*, 140, 1868
- Wu K., Kiss L. L., 2008, *A&A*, 481, 433

This paper has been typeset from a  $\text{\TeX}$ / $\text{\LaTeX}$  file prepared by the author.